
Accelerated Methods for Deep Reinforcement Learning

Adam Stooke¹ Pieter Abbeel¹

Abstract

Deep reinforcement learning (RL) has achieved many recent successes, yet experiment turn-around time remains a key bottleneck in research and in practice. We investigate how to optimize existing deep RL algorithms for modern computers, specifically for a combination of CPUs and GPUs. We confirm that both policy gradient and Q-value learning algorithms can be adapted to learn using many parallel simulator instances. We further find it possible to train using batch sizes considerably larger than are standard, without negatively affecting sample complexity or final performance. We leverage these facts to build a unified framework for parallelization that dramatically hastens experiments in both classes of algorithm. All neural network computations use GPUs, accelerating both data collection and training. Our results include using an entire NVIDIA DGX-1 to learn successful strategies in Atari games in single-digit minutes, using both synchronous and asynchronous algorithms.

1. Introduction

Research in deep reinforcement learning (RL) has relied heavily on empirical evaluation, making experiment turnaround time a key limiting factor. Despite this critical bottleneck, many reference implementations do not fulfill the potential of modern computers for throughput, unlike in supervised learning (see e.g. (Goyal et al., 2017)). In this work, we study how to adapt deep RL algorithms—without changing their underlying formulations—to better leverage multiple CPUs and GPUs. The result is a significant gain in efficiency and scale of hardware utilization and hence in learning speed.

Today’s leading deep RL algorithms have roughly clustered into two families: (i) Policy gradient methods, which rely on on-policy samples for training. A representative example is Asynchronous Advantage Actor-Critic (A3C) (Mnih et al.,

2016), in which sampler-learner processes train a centralized neural network in parallel, using only a CPU. (ii) Q-value learning methods, which permit off-policy training. A representative example is Deep Q-Networks (DQN) (Mnih et al., 2015), in which a single simulator feeds a replay buffer of transitions, and this buffer is randomly sampled for training (with a GPU). Traditionally, implementations of policy gradient methods and Q-learning methods have differed from each other; in this paper we unify them under the same framework for scaling.

Modern computers host many CPU cores and multiple GPUs on one motherboard, and we target this hardware mix. In deep RL the neural net participates both in learning and in data collection (to execute the agent’s current policy). We use GPUs for hardware acceleration of all neural network computations; to do so efficiently requires batched processing. During data collection, we run many simulator instances and batch calls to the policy or Q-function for inference. During learning, we use large batch sizes and/or asynchronous methods to expedite computation.

Our contribution is a framework for parallelized deep RL including novel techniques for GPU acceleration. Within this framework, we demonstrate multi-GPU versions of the following algorithms: Advantage Actor-Critic (Mnih et al., 2016), Proximal Policy Optimization (PPO) (Schulman et al., 2017), DQN (Mnih et al., 2015), Categorical DQN (Bellemare et al., 2017), and Rainbow (Hessel et al., 2017). Our target hardware is an NVIDIA DGX-1, which contains 40 CPU cores and 8 P100 GPUs. To provide calibrated results, we test our implementations in the heavily benchmarked Atari-2600 domain via the Arcade Learning Environment (ALE) (Bellemare et al., 2013).

We found that highly parallel sampling using batched inferences can accelerate experiment turn-around time of all algorithms without hindering training. We further found that neural networks can learn using batch sizes considerably larger than are standard, without harming sample complexity or final game score, and this dramatically speeds up learning.

The primary benefit of our implementation is improved execution speed. Our policy gradient algorithms can leverage the entire DGX-1 to learn successful game strategies in under 10 *minutes*, rather than hours. We reduced the duration

¹Department of Computer Science, University of California, Berkeley, California, USA. Correspondence to: Adam Stooke <adam.stooke@berkeley.edu>.

of some standard Q-value-learning runs from 10 days to under 2 hours. We believe that these results promise to accelerate research in deep RL, and we suggest directions for further investigation and development.

2. Related Work

Efforts to parallelize and accelerate deep RL algorithms have been underway for several years. Gorila (Nair et al., 2015) parallelized DQN using distributed computing. It achieved significant although sub-linear speedups using hundreds of computing units as samplers or learners, with central parameter servers for managing parameter updates. This effort suffered in sample complexity relative to single-threaded DQN. More recently, (Horgan et al., 2018) showed that a distributed, prioritized replay buffer can support faster learning while using hundreds of CPU cores for simulation and a single GPU for training. The same work used increased batch sizes, with a brief study of the effect of learning rate.

The policy gradient method A3C is itself a parallelized algorithm. In GA3C (Babaeizadeh et al., 2016), a speedup over CPU-only A3C was achieved by using a GPU. It was employed asynchronously, with “predictor” and “trainer” threads queuing observations and rewards for batched inferences and training updates. GA3C introduced a “policy lag” between generation and consumption of training data, worsening sample complexity. In independent work simultaneous to ours, (Espenholt et al., 2018) extended policy gradient methods to a distributed setting, enabling an alternative approach to multi-GPU training called IMPALA. They introduced a more heavily modified algorithm, *V-trace*, to mitigate policy lag—which we avoid—and did not employ GPU inference. In PAAC (Clemente et al., 2017), the authors explored the use of many simulators and increased batch sizes learning rates in (single-GPU) batched A2C—ideas central to our studies. Our contributions to actor-critic methods exceed this work in a number of ways, chiefly: improved sampling organization, tremendously enhanced scale and speed using multiple GPUs, and inclusion of asynchronous optimization.

3. RL Algorithm Background

In reinforcement learning, an agent interacts with an environment and uses the experience to optimize a decision-making policy. In a standard RL formulation, the agent aims to maximize the sum of discounted rewards, $R_t = \sum_{k=0}^{\infty} \gamma^k r_{t+k}$, in expectation, i.e. $\mathbb{E}[R_t]$. γ is the discount factor (e.g. 0.99), and r_t is the reward received at time t . The value of a state, $V(s_t) = \mathbb{E}[R_t|s_t]$, is defined as the expected discounted return from that state under a given policy, π . The Q-value, $Q(s_t, a_t) = \mathbb{E}[R_t|s_t, a_t]$ is the same but for

following the policy after first using action a_t to advance. With these definitions in hand, we briefly review the deep RL algorithms used in our experiments.

3.1. Policy Gradient Methods

In policy gradient methods, the policy is directly parameterized in the form $\pi(a|s; \theta)$, where π is a probability distribution over actions a when observing state s , as parameterized by θ , a neural network. The agent exercises the policy in the environment, recording experiences. Periodically, it uses the samples to update θ by estimating the gradient $\nabla_{\theta} \mathbb{E}[R_t]$. Typically, the agent then discards these samples and repeats, optimizing the policy iteratively.

Advantage Actor-Critic: In advantage actor-critic, the policy gradient is computed as $\mathbb{E}[\nabla_{\theta} \log \pi(a_t|s_t; \theta)(R_t - V(s_t))]$. The agent estimates $V(s_t)$ from the data, for instance using a separate output from the same network used for π . $(R_t - V_t)$ estimates the advantage: $A(s, a) = Q(s, a) - V(s)$. R_t is computed using the discounted sum of as many future returns as are observed in a given batch, up to $r_{t_{max}}$, and is bootstrapped with $V(s_{t_{max}+1})$, appropriately discounted. The estimator $V(s; \theta)$ is trained using e.g. a squared-error loss, simultaneously to π . Lastly, an entropy bonus is added to the gradient: $\nabla_{\theta} H(\pi(\cdot|s_t; \theta))$, to promote exploration and discourage premature convergence.

In A3C (Mnih et al., 2016), separate actor-learner threads sample environment steps and update a centralized copy of the parameters asynchronously to each other. In (batched) A2C, which performs similarly to A3C (see, e.g. (Schulman et al., 2017)), separate environment instances are sampled, but the learner is single-threaded. It gathers all data into one minibatch to compute the gradient.

Proximal Policy Optimization: Proximal Policy Optimization (PPO) (Schulman et al., 2017) is a closely related algorithm that improves sample complexity by increasing the training use of each sample. It maximizes a “surrogate” objective $\mathbb{E}[\rho_t(\theta)A_t]$, where $\rho_t(\theta) = \pi(a_t|s_t; \theta)/\pi(a_t|s_t; \theta_{old})$ is the likelihood ratio of the recorded action between the updated and original policies. We use the clipping-objective version of PPO, which optimizes the expression $\mathbb{E}[\min(\rho_t(\theta)A_t, \text{clip}(\rho_t(\theta), 1 - \epsilon, 1 + \epsilon)A_t)]$, noting that $\rho_t(\theta_{old}) = 1$. Unlike A3C, PPO performs multiple parameter updates using (minibatches from) each set of samples; the clipping objective prevents excessive policy updates from destabilizing learning.

3.2. Q-Value-Learning Methods

Instead of directly parameterizing a policy, Q-value learning methods estimate the Q-function as $Q(s, a; \theta)$. The greedy

policy selects the (discrete) action maximizing value: $a^* = \operatorname{argmax}_a Q(s, a; \theta)$. Exploration can be performed using an ϵ -greedy policy, which chooses a uniform random action with probability ϵ and otherwise uses the greedy action. By its off-policy nature, Q-learning permits repeated training use of samples.

Deep Q-Networks: Deep Q-Networks (DQN) (Mnih et al., 2015) optimize the Q-value estimator by repeated gradient descent on the objective: $\mathbb{E} [(y_i - Q(s_i, a_i; \theta))^2]$, where y_i is the data-estimated Q-value given by $y_i = r_i + \gamma \max_a Q(s_{i+1}, a; \theta^-)$ (although in practice the Huber loss is used). DQN gains stability by 1) using a separate “target” network θ^- , periodically copied from θ , and 2) training from a replay buffer, to which it continually adds new experiences. Several enhancements to DQN have improved performance.

Categorical DQN: Categorical DQN (Bellemare et al., 2017) discretizes the possible Q-values into a fixed range and number of “atoms” and learns a distribution for each $Q(s, a; \theta)$, so as to represent stochastic features of the environment. The squared-error loss function is replaced by the Kullback-Leibler divergence against a target distribution. The target is constructed by contracting the “future” atoms according to γ and shifting them by R_t . Action-selection is still performed greedily according to expected value over the distribution.

ϵ -Rainbow: Recently, the use of distributional learning was combined with five other enhancements to DQN under a single name: Rainbow (Hessel et al., 2017). Without describing them here, the enhancements include: 1) Double-DQN (Van Hasselt et al., 2016), 2) Dueling Networks (Wang et al., 2016), 3) Prioritized Replay (Schaul et al., 2016), 4) n-step learning (Peng & Williams, 1994), and 5) NoisyNets (Fortunato et al., 2018). In our experiments, we use the ϵ -greedy version of Rainbow, without parameter noise.

4. Parallel, Accelerated RL Framework

We consider learning scenarios where the environment is a CPU-based simulator and the policy uses a deep neural network. We describe here a complete set of parallelization techniques that achieve high throughput during both sampling and optimization. It is applicable to many deep RL algorithms, including those outlined above. We treat GPUs homogeneously; each performs the same sampling-learning procedure. This strategy scales straightforwardly to various numbers of GPUs.

4.1. Synchronized Sampling

We begin by associating multiple CPU cores with a single GPU. We run multiple simulators in parallel processes on

the CPU cores, and these processes perform environment steps in a synchronized fashion. At each step, all individual observations are gathered into a batch for inference, which is called on the GPU once the last observation is submitted. The simulators step again once the actions are returned, and so on, as in (Clemente et al., 2017). System shared memory arrays provide fast communication between the action-server and simulator processes.

The number of CPU cores might limit the inference batch size, so we use multiple simulator instances per process. These are stepped sequentially (within each process) and always all together in every inference batch. This arrangement adds the benefit that it mitigates synchronization losses. Variance in simulator stepping time arises from differing simulator states and other random fluctuations. The straggler effect worsens with increased number of parallel processes but diminishes with increased number of sequential simulators. A schematic is shown in Figure 1. Slowdowns caused by long environment resets can be avoided by resetting only during optimization pauses.¹

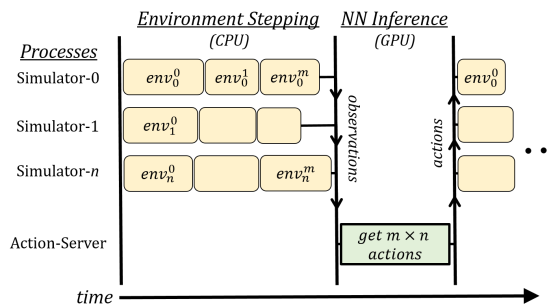


Figure 1. Synchronized sampling schematic, showing multiple simulator processes, each with multiple simulator instances, interacting synchronously with a GPU-based action-server through time (alternating scheme not shown).

When running this sampling engine, hardware component utilization reflects the relative load of each side of computation. If simulation and inference loads are balanced, this would cause each component to sit idle half of the time. We avoid this idleness by forming two alternating groups of simulator processes. While one group awaits an inference, the other steps, and the GPU alternates between servicing each group. Alternation keeps utilization high; moreover, it hides the execution time of whichever computation is the quicker of the two.

We found it beneficial to fix the CPU assignment of each simulator process. To use multiple GPUs, we simply repeat the template, allocating available CPU cores evenly. We have found it sufficient to reserve one CPU core to run each

¹For example, one may either 1) ignore a simulator in need of reset or 2) immediately swap in a fresh instance held in reserve.

GPU. The experiments section contains measurements of sampling speed, which indeed increases with the number of environment instances.

4.2. Synchronous Multi-GPU Optimization

In our synchronous algorithms, all GPUs maintain identical parameter values. We leverage the data-parallelism of stochastic gradient estimation and use the well-known update procedure, on every GPU: 1) compute a gradient using locally-collected samples, 2) all-reduce the gradient across GPUs, 3) use the combined gradient to update local parameters. We use the NVIDIA Collective Communication Library for fast communication among GPUs.

4.3. Asynchronous Multi-GPU Optimization

In asynchronous optimization, each GPU acts as its own sampler-learner unit and applies updates to a central parameter store held in CPU memory. The training batch size does not aggregate across GPUs, thus avoiding a potential limit to scaling.

Use of accelerators compels a choice of where to perform the parameter update. In our experience, applying common update rules to the network is faster on the GPU. Our general update procedure includes three steps: 1) compute the gradient locally and store it on the GPU, 2) pull current central parameters onto the GPU and apply the update rule to them using the pre-computed gradient, 3) write the updated parameters back to the central store. After this sequence, the local GPU parameters are in sync with the central values, and sampling proceeds again. Following (Mnih et al., 2016), we centralize the update rule parameters in addition to the network weights.

Rather than add update increments to the central parameters, which requires CPU computation, we overwrite the values. Therefore, we employ a lock around steps (2) and (3) above, preventing other processes from reading or writing parameter values concurrently. Typically, we divide the parameters into a small number of disjoint chunks which are updated separately, each with its own lock (steps 2-3 become a loop over chunks). This balances update call efficiency against lock contention and can provide good performance. When large intermediate updates occur, it can be beneficial to pull the central network weights more frequently (e.g. during sampling and/or before gradient computation). In the surrogate loss of PPO, we use the action probabilities experienced during sampling.

5. Experiments

We used the Atari-2600 domain to study the scaling characteristics of highly parallelized RL, addressing the following: 1) How efficient is our synchronized sampling engine, and

what speeds can it achieve? 2) Can policy gradient and Q-learning algorithms be adapted to learn using many parallel simulator instances without diminishing learning performance? 3) Can large-batch training and/or asynchronous methods speed up optimization without worsening sample complexity?

In all learning experiments, we maintained the original *training intensity*—meaning average number of training uses of each sampled data point. For A3C, PPO, and DQN+variants, the reference training intensities are 1, 4, and 8, respectively.

All learning curves shown here are averages over at least two random seeds. For policy gradient methods, we tracked online scores, averaging over the most recent 100 completed trajectories. For DQN and variants, we paused every 1-million steps to evaluate for up to 125,000 steps, with maximum path length of 27,000 steps, as is standard. The appendices contain learning curves beyond those we highlight here.

5.1. Atari Frame Processing

Our frame pre-processing closely resembles that originally described in (Mnih et al., 2015). The sole difference is that we abandon the square frame dimensions in favor of simply downsizing by a factor of 2, which provides crisp images at minimal computational cost. Before downsizing, we crop two rows, making the final image size 104×80 . This simplifies selection of convolution size, stride, and padding. Otherwise, we kept all standard settings. For Q-learning experiments, we used the 3-convolutional-layer network as in (Mnih et al., 2015) (DQN-Net) or its algorithm-specific variants, and for policy gradients the 2-convolutional-layer feed-forward network of (Mnih et al., 2016) (A3C-Net). The second (and third) convolution layers have padding 1, so the convolution output is always 25×19 .

5.2. Sampling

A series of sampling-only measurements demonstrated that despite the potential for stragglers, the synchronized sampling scheme can achieve good hardware utilization.

First, we studied the capacity of a single GPU at serving inferences for multiple environments. Figure 2 shows measurements running a trained A3C-Net policy on a P100 GPU while playing the game BREAKOUT. Aggregate sampling speed, normalized by CPU core count, is plotted as a function of the number of (sequential) Atari simulators running on each core.² The minimum was 2 simulators per core by the alternating scheme. Different curves represent different numbers of CPU cores running simulations. For reference, we include the sampling speed of a single core

²Intel TurboBoost was disabled for this test only, keeping the clock speed of every core at 2.2 GHz.

Table 1. Sampling speeds on the DGX-1 with A3C-Net, by total simulator count, in thousands of samples per second.

# SIMS (PER CORE)	SYNC	ASYNC
64 (2)	29.6	31.9
128 (4)	33.0	34.7
256 (8)	35.7	36.7
512 (16)	35.8	38.4

running without inference—the dashed line for a single process, and the dotted line one process on each of the two Hyperthreads. Running with inferences and with a single core, the sampling speed increased with simulator count until the inference time was completely hidden. Synchronization losses appeared for higher core count. But at as little as 8 environments per core, the GPU supported even 16 CPU cores running at roughly 80% of the inference-free speed.

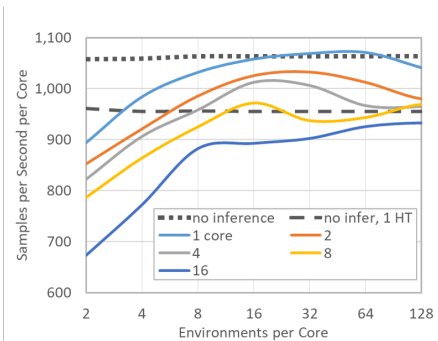


Figure 2. Sampling speed vs number of simulators per core, playing BREAKOUT using 1 GPU. Curves are by number of cores performing simulations. Running multiple simulators per core mitigates synchronization losses and hides NN inference time, resulting in high throughput.

Next, we measured the sampling-only speed of the same A3C-Net playing BREAKOUT parallelized across an entire NVIDIA DGX-1. Table 1 shows results for various total simulator counts. In the synchronized setting, a barrier was placed across all GPU processes every five steps (mimicking the optimization in A2C). Otherwise, each GPU and its associated cores ran independently. At simulator counts of 256 (8 per core) and above, our sampling engine achieved greater than 35,000 samples per second. This equates to 500 million emulator frames per hour, possibly the fastest reported Atari sampling rate using a single computer.

5.3. Learning with Many Simulator Instances

To leverage the high throughput of parallel sampling, we attempted to adapt existing deep RL algorithms to learn with many simulator instances. The following results show that indeed all algorithms we considered can be adapted without losing performance, and with only minor changes. We experimented with different techniques for each algorithm,

which we describe and evaluate here. Interestingly, scaling affects synchronous and asynchronous learning somewhat differently, looking across games.

A2C: We experimented with A2C by letting the optimization batch size grow with the number of simulators while keeping the sampling horizon fixed (at 5 steps as in A3C). Correspondingly fewer parameter update steps were made per sample gathered. Unlike in (Clemente et al., 2017), we empirically determined that increasing the learning rate with the *square root* of the batch size worked best. A gradual decay in efficiency remained. The top panel of Figure 3 shows learning curves vs total sample count for a test set of games, with simulator count ranging from 16 to 512 (batch size 80 to 2,560). We used RMSProp with a base learning rate of 7×10^{-4} (scaled up to 3×10^{-3} here).

A3C: An asynchronous adaptation we experimented with used a 16-environment A2C agent as the base sampler-learner unit. Figure 3 shows learning curves vs aggregate sample count for numbers of learners ranging from 1 to 32,³ corresponding to 16 to 512 total simulators. We found no hyperparameter adjustments to be necessary. The resulting learning curves were nearly indistinguishable in most cases, although some did degrade at the largest scales.

PPO: The large batch size already used to benchmark PPO (8-simulator x 256-horizon = 2,048) provided a different route to using many simulators. We adapted PPO by decreasing the sampling horizon such that the total batch size remained fixed. Figure 3 shows learning curves vs sample count for simulator counts ranging from 8 to 512, with corresponding sampling horizons ranging from 256 down to 4 steps. We changed no optimization settings. Learning improved or worsened slightly on some test games.

APPO: We also experimented with an asynchronous version of PPO. We used an 8-simulator PPO agent as the base learner unit, using the same sampling horizon and update sequence as original PPO. The bottom panel in Figure 3 shows learning curves from a study of 8 learners running on 8 GPUs, with varying communication frequency. Standard PPO uses 4 gradient updates per epoch, and 4 epochs per optimization; we experimented with 1-4 gradient updates between synchronizations (update rule provided in supplementary material). Relative to PPO, we introduced gradient-norm-clipping, reduced the learning rate by a factor of four, and removed the learning rate schedule, all of which benefited learning. We found it helpful to periodically pull the central policy parameters during sampling, and did this with a horizon of 64 steps in all cases. In several games, the learning remained fairly consistent; it may be possible to reduce communication in asynchronous settings.

³Learner counts in excess of 8 were run with multiple separate learners sharing GPUs.

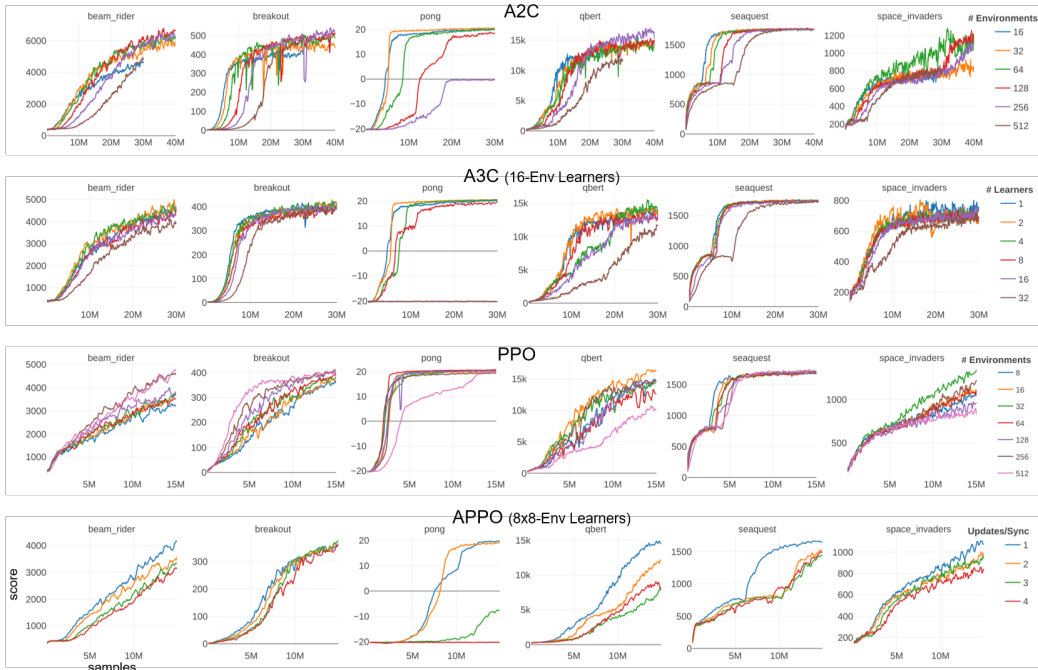


Figure 3. Scaling investigations for policy gradient algorithms: game scores vs aggregate sample count. Top) A2C with various batch sizes (proportional to environment count), Upper) A3C with various numbers of 16-environment learner processes, Lower) PPO with varied number of simulators, Bottom) Asynchronous PPO, 8 learners with varied communication period. In most but not all cases, the scaled/adapted versions match the baseline performance.

DQN + Variants: To adapt DQN and variants to run with many simulator instances, we performed learning experiments using an experience replay buffer organized by simulator. The total buffer size remained at 1 million transitions, so a correspondingly shorter history was held for each simulator. We observed learning performance to be largely independent of simulator count up to over 200, provided the number of update steps per optimization cycle is not too high (large batch size ameliorates this).

Start State Decorrelation: Learning failed very early in some many-simulator experiments. We attributed this to correlation in starting game states, which resulted in large but poorly informed learning signals. To correct this, all our experiments start by stepping every simulator through a random number of uniform-random actions. Once this measure is taken, we found learning rate warmup (Goyal et al., 2017) to have no effect. On commencing sampling for training, game resets proceed as usual.

5.4. Q-Value Learning with Large Training Batches

We performed experiments to explore the effects of training batch size in Q-value learning. They confirm that sample-efficient, large-batch training is possible with DQN. Further, we begin to shed light on the optimization effects of batch size.

5.4.1. ALGORITHM PERFORMANCE

DQN: When growing the simulator count and batch size in DQN, we maintained training intensity by adjusting the sampling horizon and the number of update steps per optimization phase. We experimented with batch sizes ranging from the standard 32 up to 2,048, and found consistent learning performance up to 512. Beyond this batch size, it became increasingly difficult to find a single learning rate which performed well in all tested games, and some maximum scores suffered. Figure 4 shows DQN learning performance for the batch sizes 32, 512, and 1024, using learning rates $2.5, 7.5, 15 \times 10^{-4}$, respectively. Other hyperparameters were as in original DQN (Mnih et al., 2015). In several games, a larger batch size improved learning. We also found asynchronous DQN to learn well using up to 4 GPU learners, each using batch size 512, with no further adjustments.

Categorical DQN: We found Categorical DQN to scale further than DQN. The lower panel of Figure 4 shows learning curves for batch sizes up to 2,048, with no diminution in maximum scores. This is possibly due to richer content of the gradient signal. We employed the published setting for epsilon in the Adam optimizer: $0.01/L$, where L is the batch size. Notably, learning was delayed for the largest batch sizes in the game SEAQUEST, but greater maximum

scores were eventually reached. In contrast to previous algorithms, we found a single learning rate to apply broadly, using 4.2×10^{-4} at all batch sizes of 256 and above. We return to study this surprising result shortly.

ϵ -Rainbow: Despite its use of distributional learning, we found ϵ -Rainbow to lose performance above batch size 512 in some games. Scores for batch size 512 appear in Figure 12 in an appendix. They roughly match (in some cases exceeding) those reported in the literature for batch size 32 (Hessel et al., 2017). We used the published hyperparameters without scaling the learning rate. We scaled epsilon in the Adam update rule as $0.005/L$, with L the batch size.

5.4.2. EFFECTS OF BATCH SIZE ON OPTIMIZATION

Some possible factors limiting training batch sizes include: 1) reduced exploration, since fewer different networks are exercised in the environment, and 2) difficulties in numerical optimization of network weights. We conducted experiments to begin to identify these factors.

Secondary-Learner Experiment: We configured a secondary DQN learner to train using only the replay buffer of a normal DQN agent. The secondary learner was initialized with the same parameter values as the primary, “sampler-learner”, and the two networks trained simultaneously, at the same rate of data consumption. Each sampled its own training batches. In the game of BREAKOUT, 64- and 2048-sampler-learners achieved the same score, but the 2048-learner required more samples, despite using the fastest stable learning rate (the number refers to training batch size). When training a 64-secondary-learner using a 2048-sampler-learner, the secondary learner’s score tracked that of the primary. In the reverse scenario, however, the 2048-secondary-learner failed to learn. We posit this was due to the slower optimization of the decreased number of parameter updates—it was unable to track the rapid changes to the Q-value estimates near initialization and became too off-policy to learn. In the same test using two 256-learners, their scores matched. Had the 2048-secondary-learner outpaced the 2048-sampler-learner, it would have suggested exploration to be a more important factor than optimization. See the supplementary materials for figures.

Update Rule: We conducted another experiment to isolate the effect of update rule on optimization. We found the Adam (Kingma & Ba, 2014) formula to be superior to RMSProp (Tieleman & Hinton) in providing large-batch learners with capability to traverse parameter-space during learning. When comparing learners achieving the same learning curves, those using smaller batch sizes (and hence performing more update steps) tended to have larger parameter vector-norms at all points in training. Unlike RMSProp, the Adam rule resulted in a fairly tight spread in parameter norms between batch sizes without changing the learning

Table 2. Hours to complete 50 million steps in policy gradient learning on the DGX-1, by GPU count. A2C/A3C used 16 environments per GPU, PPO/APPO used 8.

ALGORITHM	# GPU (# CPU)			
	1 (5)	2 (10)	4 (20)	8 (40)
A2C	3.8	2.2	1.2	0.59
A3C	–	2.4	1.3	0.65
PPO	4.4	2.6	1.5	1.1
APPO	–	2.8	1.5	0.71

rate. This explains the lack of need to scale the learning rate in Categorical DQN and ϵ -Rainbow, and indicates that the update rule plays an important role in scaling. Further details, including differences in trends between convolutional and fully connected layers, appear in an appendix.

5.5. Learning Speed

Finally, we demonstrated the learning speeds our framework obtains when running an entire DGX-1 to learn a single game. Figure 5 shows results for well-performing configurations of the policy gradient methods A2C, A3C, PPO, and APPO. Several games exhibit a steep initial learning phase; all algorithms here completed that phase in under 10 minutes in all such games shown. Notably, PPO mastered Pong in 4 minutes. A2C with 256 environments reached a processing speed in excess of 25,000 samples per second, equating to over 90 million steps per hour (360 million frames). Scaling measurements are listed in Table 2, showing in excess of 6x speedup using 8 GPUs relative to 1.

We ran synchronous versions of DQN and its variants, with training times shown in Table 3. Using 1 GPU and 5 CPU cores, DQN and ϵ -Rainbow completed 50 million steps (200 million frames) in 8 and 14 hours, respectively—a significant gain over the reference times of 10 days. We achieved comparable learning speeds to those in (Horgan et al., 2018), which used 1 GPU and 376 CPU cores (see e.g. Figure 2 therein for 10-hour learning curves). Using multiple GPUs and more cores sped up our implementations. By virtue of a larger batch size, Categorical-DQN scaled best and completed training in under 2 hours using the entire DGX-1, a speedup of over 6x relative to 1 GPU. DQN and ϵ -Rainbow, however, experienced diminishing returns beyond 2 GPUs. We were unable to find asynchronous configurations that further boosted learning speed without curbing performance in some games (we only tested fully-communicating algorithms). Opportunities may exist to improve on our scaling.

6. Conclusions and Discussion

We have introduced a unified framework for parallelizing deep RL that uses hardware accelerators to achieve fast learning. The framework is applicable to a range of al-

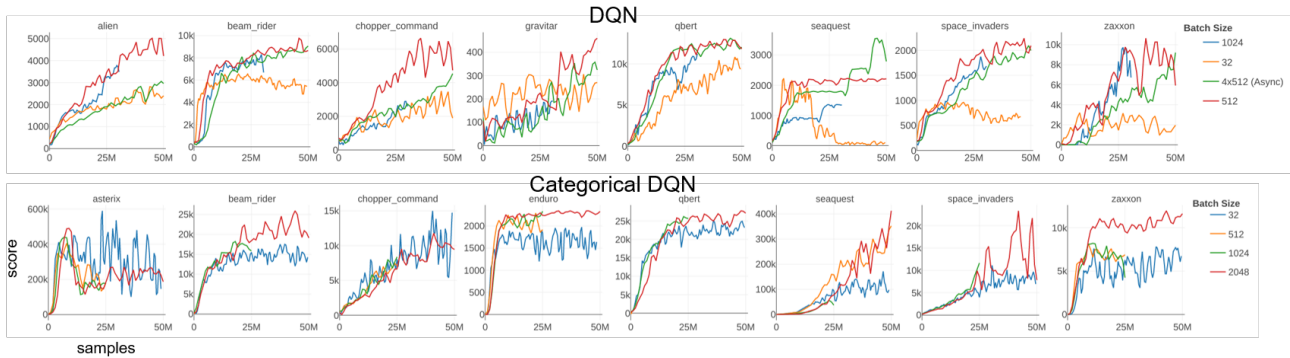


Figure 4. Scaling investigations for DQN (top) and Categorical-DQN (bottom): game scores vs sample count. Both learn well using training batch sizes as large as 512; Categorical-DQN succeeds using up to 2,048.

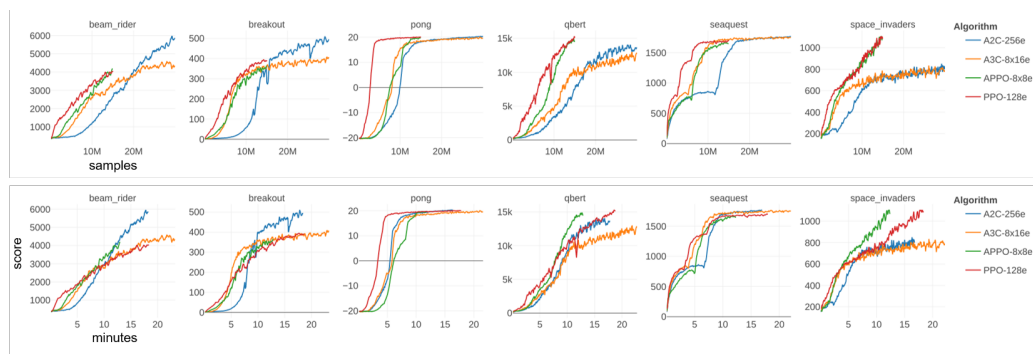


Figure 5. Policy gradient algorithms using an entire DGX-1 for a single learning run: game scores vs aggregate sample count and vs time, in minutes. Asynchronous and synchronous versions of A2C and PPO learn successful game strategies in under 10 minutes.

Table 3. Hours to complete 50 million steps (200 million frames) in Q-learning on the DGX-1, by GPU count (synchronous).

ALGORITHM-B.S.	# GPU (# CPU)			
	1 (5)	2 (10)	4 (20)	8 (40)
DQN-512	8.3	4.8	3.1/3.9*	2.6
ϵ -RAINBOW-512	14.1	8.6	6.6	6.4
CAT-DQN-2048	10.7	6.0	2.8	1.8

* Asynchronous

gorithms, including policy-gradient and Q-value learning methods. Our experiments show that several leading algorithms can learn a variety of Atari games in highly parallel fashion, without loss of sample complexity and at unprecedented wall-clock times. This result indicates a promising direction to significantly boost experiment scale. We will release the code-base.

We note several directions for extension of this framework. First is to apply it to domains other than Atari, especially ones involving perception. Second, our framework is likely to scale favorably to more sophisticated neural network agents, due to GPU acceleration of both inference

and training. Moreover, as network complexity increases, scaling could become easier, as GPUs may run efficiently with smaller batch sizes, although communication overhead would worsen. Reduced-precision arithmetic could hasten learning—a topic yet to be explored in deep RL due to use of CPU-based inference. Larger RL problems may use the current, single-node implementation as a building block for distributed algorithms.

Questions remain as to the extent of parallelization possible in deep RL. We have not conclusively identified the limiting factor to scaling, nor if it is the same in every game and algorithm. Although we have seen optimization effects in large-batch learning, we do not know their full nature, and other factors remain possible. Limits to asynchronous scaling remain unexplored; we did not definitively determine the best configurations of these algorithms, but only presented some successful versions. Better understanding may enable further gains in scaling, which is a promising direction for the advancement of deep RL.

Acknowledgements

Adam Stooke gratefully acknowledges the support of the Fannie & John Hertz Foundation. The DGX-1 used for this research was donated by the NVIDIA Corporation. We thank Frédéric Bastien and the Theano development team (Theano Development Team, 2016) for their framework and helpful discussions during development of GPU-related methods. Thanks to Rocky Duan *et al* for the *rllab* codebase (Duan *et al.*, 2016) out of which this work evolved.

References

- Babaeizadeh, Mohammad, Frosio, Iuri, Tyree, Stephen, Clemons, Jason, and Kautz, Jan. GA3C: gpu-based A3C for deep reinforcement learning. *arXiv preprint arXiv: 1611.06256*, 2016.
- Bellemare, Marc G, Naddaf, Yavar, Veness, Joel, and Bowling, Michael. The arcade learning environment: An evaluation platform for general agents. *Journal of Artificial Intelligence Res.*, 47:253–279, 2013.
- Bellemare, Marc G, Dabney, Will, and Munos, Rémi. A distributional perspective on reinforcement learning. *arXiv preprint arXiv: 1707.06887*, 2017.
- Clemente, Alfredo V., Martínez, Humberto Nicolás Castejón, and Chandra, Arjun. Efficient parallel methods for deep reinforcement learning. *CoRR*, abs/1705.04862, 2017. URL <http://arxiv.org/abs/1705.04862>.
- Duan, Yan, Chen, Xi, Houthoofd, Rein, Schulman, John, and Abbeel, Pieter. Benchmarking deep reinforcement learning for continuous control. *CoRR*, abs/1604.06778, 2016. URL <http://arxiv.org/abs/1604.06778>.
- Espeholt, L., Soyer, H., Munos, R., Simonyan, K., Mnih, V., Ward, T., Doron, Y., Firoiu, V., Harley, T., Dunning, I., Legg, S., and Kavukcuoglu, K. IMPALA: Scalable Distributed Deep-RL with Importance Weighted Actor-Learner Architectures. *ArXiv e-prints*, February 2018.
- Fortunato, Meire, Azar, Mohammad Gheshlaghi, Piot, Bilal, Menick, Jacob, Hessel, Matteo, Osband, Ian, Graves, Alex, Mnih, Volodymyr, Munos, Remi, Hassabis, Demis, Pietquin, Olivier, Blundell, Charles, and Legg, Shane. Noisy networks for exploration. In *International Conference on Learning Representations*, 2018.
- Goyal, Priya, Dollr, Piotr, Girshick, Ross, Noordhuis, Pieter, Wesolowski, Lukasz, Kyrola, Aapo, Tulloch, Andrew, Jia, Yangqing, and He, Kaiming. Accurate, large minibatch sgd: Training imagenet in 1 hour, 2017.
- Hessel, Matteo, Modayil, Joseph, van Hasselt, Hado, Schaul, Tom, Ostrovski, Georg, Dabney, Will, Horgan, Dan, Piot, Bilal, Azar, Mohammad, and Silver, David. Rainbow: Combining improvements in deep reinforcement learning. *arXiv preprint arXiv: 1710.02298*, 2017.
- Horgan, D., Quan, J., Budden, D., Barth-Maron, G., Hessel, M., van Hasselt, H., and Silver, D. Distributed Prioritized Experience Replay. *ArXiv e-prints*, March 2018.
- Kingma, Diederik P. and Ba, Jimmy. Adam: A method for stochastic optimization. *CoRR*, abs/1412.6980, 2014. URL <http://arxiv.org/abs/1412.6980>.
- Mnih, Volodymyr, Kavukcuoglu, Koray, Silver, David, Rusu, Andrei A, Veness, Joel, Bellemare, Marc G, Graves, Alex, Riedmiller, Martin, Fidjeland, Andreas K, Ostrovski, Georg, Petersen, Stig, Beattie, Charles, Sadik, Amir, Antonoglou, Ioannis, King, Helen, Kumaran, Dharshan, Wierstra, Daan, Legg, Shane, and Hassabis, Demis. Human-level control through deep reinforcement learning. *Nature*, 518(7540):529–533, 2015.
- Mnih, Volodymyr, Badia, Adrià Puigdomènech, Mirza, Mehdi, Graves, Alex, Lillicrap, Timothy P, Harley, Tim, Silver, David, and Kavukcuoglu, Koray. Asynchronous methods for deep reinforcement learning. In *International Conference in Machine Learning*, 2016.
- Nair, Arun, Srinivasan, Praveen, Blackwell, Sam, Alciçek, Cagdas, Fearon, Rory, De Maria, Alessandro, Panneershelvam, Vedavyas, Suleyman, Mustafa, Beattie, Charles, Petersen, Stig, Legg, Shane, Mnih, Volodymyr, Kavukcuoglu, Koray, and Silver, David. Massively parallel methods for deep reinforcement learning. *arXiv preprint arXiv: 1507.04296*, 2015.
- Peng, Jing and Williams, Ronald J. Incremental multi-step q-learning. In *Machine Learning Proceedings 1994*, pp. 226–232. Elsevier, 1994.
- Schaul, Tom, Quan, John, Antonoglou, Ioannis, and Silver, David. Prioritized experience replay. In *International Conference on Learning Representations*, 2016.
- Schulman, John, Wolski, Filip, Dhariwal, Prafulla, Radford, Alec, and Klimov, Oleg. Proximal policy optimization algorithms. *arXiv preprint arXiv: 1707.06347*, 2017.
- Theano Development Team. Theano: A Python framework for fast computation of mathematical expressions. *arXiv e-prints*, abs/1605.02688, May 2016. URL <http://arxiv.org/abs/1605.02688>.
- Tieleman, T. and Hinton, G. RMSprop Gradient Optimization. URL http://www.cs.toronto.edu/~{}tijmen/csc321/slides/lecture_slides_lec6.pdf.

Van Hasselt, Hado, Guez, Arthur, and Silver, David. Deep reinforcement learning with double q-learning. In *AAAI*, volume 16, pp. 2094–2100, 2016.

Wang, Ziyu, Schaul, Tom, Hessel, Matteo, van Hasselt, Hado, Lanctot, Marc, and de Freitas, Nando. Dueling network architectures for deep reinforcement learning. In *International Conference on Machine Learning*, 2016.

Supplementary Materials

A. Update Rule for Multi-Step Asynchronous Adam

Our asynchronous PPO experiments used the update rule described here, which permits multiple local gradient steps per synchronization with the central parameters. The usual Adam update rule (Kingma & Ba, 2014) is the following. It has fixed hyperparameters r , β_1 , β_2 , and ϵ ; g stands for the gradient; and all other values except the network parameters θ are initialized at 0:

$$\begin{aligned}
 t &\leftarrow t + 1 \\
 a &\leftarrow r \frac{\sqrt{1 - \beta_2^t}}{1 - \beta_1^t} \\
 m &\leftarrow \beta_1 m + (1 - \beta_1)g \\
 v &\leftarrow \beta_2 v + (1 - \beta_2)g^2 \\
 s &\leftarrow \frac{am}{\sqrt{v\epsilon}} \\
 \theta &\leftarrow \theta - s \quad .
 \end{aligned}$$

We kept these rules for making local updates and introduced the additional, local accumulation variables, also zero-initialized:

$$\begin{aligned}
 a_g &\leftarrow \beta_1 a_g + g \\
 a_{g^2} &\leftarrow \beta_2 a_{g^2} + g^2 \\
 a_s &\leftarrow a_s + s \quad .
 \end{aligned}$$

When applying an update to the central parameters, denoted with a tilde, we used the following assignments:

$$\begin{aligned}
 \theta, \tilde{\theta} &\leftarrow \tilde{\theta} - a_s \\
 m, \tilde{m} &\leftarrow \beta_1^n \tilde{m} + (1 - \beta_1)a_g \\
 v, \tilde{v} &\leftarrow \beta_2^n \tilde{v} + (1 - \beta_2)a_{g^2} \\
 a_g, a_{g^2}, a_s &\leftarrow 0
 \end{aligned}$$

where n is the number of local gradient steps taken between synchronizations. This rule reduces to the usual Adam update rule in the case of a single learner thread.

B. Figures for Secondary-Learner Experiment (DQN)

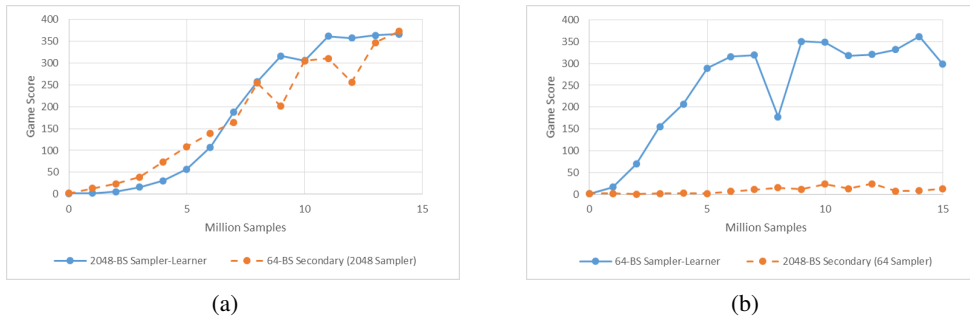


Figure 6. Learning the game BREAKOUT with a secondary-learner using only the replay buffer of the normal, sampler-learner, both using DQN. a) The 64-batch-size secondary-learner kept pace with its 2048-batch-size sampler-learner, but b) the 2048-batch-size secondary learner failed to track its 64-batch-size sampler-learner or even learn at all. (Curves averaged over two random trials.)

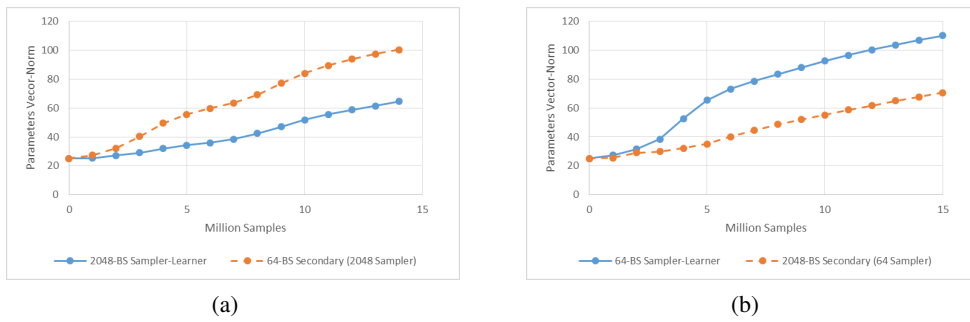


Figure 7. Neural network parameter vector-norms ($l=2$) during training. In both cases, the large-batch learner lagged behind the small batch learner. In b) the parameters of large-batch secondary-learner continued to grow while its game score remained nil.

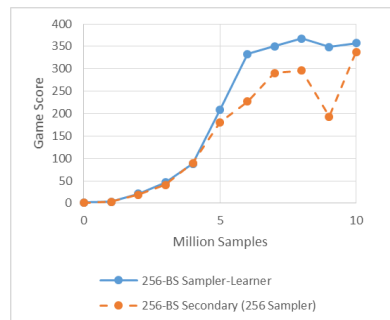


Figure 8. Learning the game BREAKOUT, where a secondary-learner using the same batch-size as the sampler-learner tracked (albeit imperfectly) the game score, learning successfully. (Curves averaged over two random trials.)

C. Observations on Update Rules and Batch Size Scaling

We present observations of the effects of scaling the training batch size on neural net optimization under two different parameter update rules: Adam and RMSProp (RMSProp without momentum and only direct accumulation of the squared gradients, see e.g. <https://github.com/Lasagne/Lasagne/blob/master/lasagne/updates.py>). We trained agents on the game Q*BERT with learning rates adjusted to yield very similar performance curves for all settings, and we tracked the L_2 vector-norms of several quantities during learning. These included the gradients, parameter update steps, and the parameter values themselves. As in all DQN experiments in this paper, the training intensity was fixed at 8, so that the number of parameter update steps during learning scaled inversely with the batch size. Two random seeds were run for each setting.

Although the game scores roughly matched throughout training, the exact solutions found at any point did not, as evidenced by the differing parameter norms. No regularization was used. The following paragraphs follow the panels in Figure 9, where curves are labeled by batch-size and learning rate. When viewing the network as a whole (i.e. norms of all weights and biases as a single vector), trends reflected those seen in FC-0, where most of the weights are.

i) Learning Curves: We controlled for game score, adjusting the learning rate as needed. For the case of RMSProp with batch-size 64, we included a learning rate that was slightly too low (1×10^{-4}), yielding slow learning and lower final score, and a learning rate that was slightly too high (5×10^{-4}), yielding lower final score due to instability—these are the dashed lines in all panels.

ii) Fully-Connected-0 Weights-Norm: The Adam optimizer yielded fairly tight grouping despite using the same learning rate for all settings. The RMSProp learner, on the other hand, needed to scale the learning rate by 20x between batch sizes 64 and 1,024, which then produced very similar norms. At batch-size 64, slow / unstable learning was characterized by small / large norms, respectively. The large norm of the batch-size 256 runs suggests this learning rate was likely near the upper limit of stability.

iii) Fully-Connected-0 Gradients-Norm: Under both update rules, large batch sizes always produced smaller gradient vectors—reduced variance led to reduced magnitudes. We also observed this pattern in policy gradient methods, when looking at the total gradient norm. Here, the magnitude of the gradients depended inversely on the parameter norm; see the RMSProp 64-batch-size curves. This effect was opposed and outweighed by the effect of batch size.

iv) Fully-Connected-0 Step-Norm: The Adam optimizer yielded significantly bigger step sizes for the bigger batch learners, despite the smaller gradients. RMSProp required an adjusted learning rate to produce the same effect. Under both update rules, the amount of step size increase did not fully compensate for the reduction in step count, indicating that the larger batch learners followed straighter trajectories through parameter space. RMSProp led to significantly larger steps overall, but despite this ended learning at smaller weights—its learning trajectories were apparently less direct, more meandering.

v) Convolution-0 Weights-Norm: The Adam optimizer gave much greater spread in norms here than in the FC-0 layer; as batch size increased, the learning emphasis shifted away from Conv-0. But in RMSProp the increased learning rate led the first convolution layer to grow larger for larger batch sizes, placing more emphasis on this layer.

vi) Convolution-0 Gradients-Norm: The Adam update rule produced an intriguing cross-over in gradient norm; the large batch learner actually started higher, bucking the trend seen in other cases. The pattern under RMSProp matched that for FC-0.

vii) Convolution-0 Step-Norm: Unlike for FC-0, the step norm did not change significantly with batch size under Adam. RMSProp yielded a similar pattern as in FC-0.

Overall, the Adam optimizer appeared to compensate for batch size in the FC-0 layer, but less so in the Conv-0 layer, leading to de-emphasized learning in Conv-0 for large batches. The increased learning rate in RMSProp compensated for batch size in the FC-0 layer and *increased* the emphasis on learning in Conv-0. This sort of pattern could have implications for learning representations vs game strategies. Further study of these clear trends could yield insights into the causes of learning degradation and possible solutions for large batch RL.

Accelerated Methods for Deep Reinforcement Learning

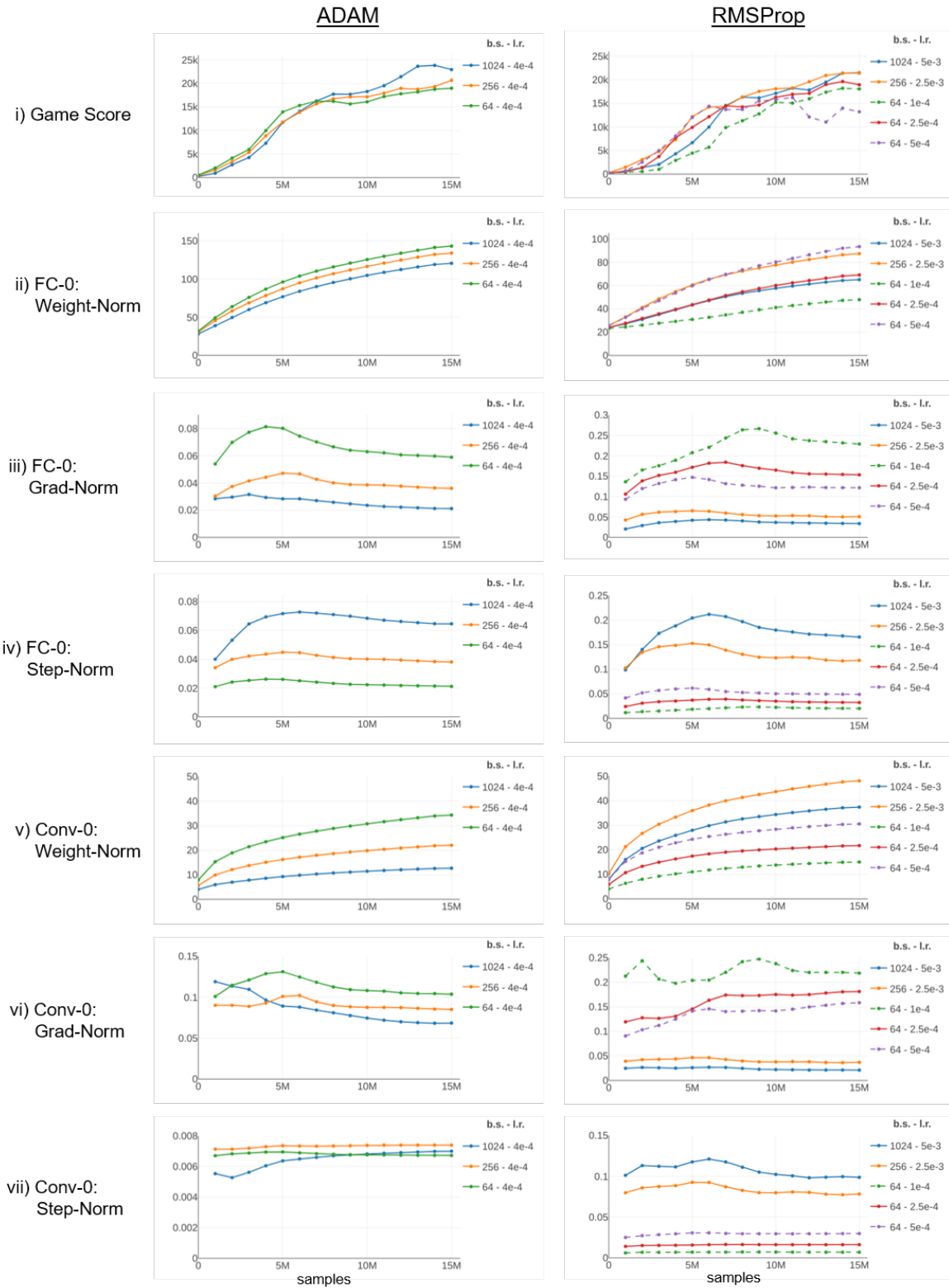


Figure 9. L-2 vector-norms of the parameters, gradients (average), and parameter steps (average) for the first convolution layer and the first fully connected layer while learning to play Q*BERT with Categorical DQN at various batch sizes: Adam vs RMSProp.

D. Additional Learning Curves



Figure 10. Learning curves for Advantage Actor-Critic: baseline (A2C-16env) and scaled configurations, including synchronous and asynchronous. Only in ATLANTIS, GOPHER, and possibly KRULL does the baseline stand out above both scaled versions.

Accelerated Methods for Deep Reinforcement Learning

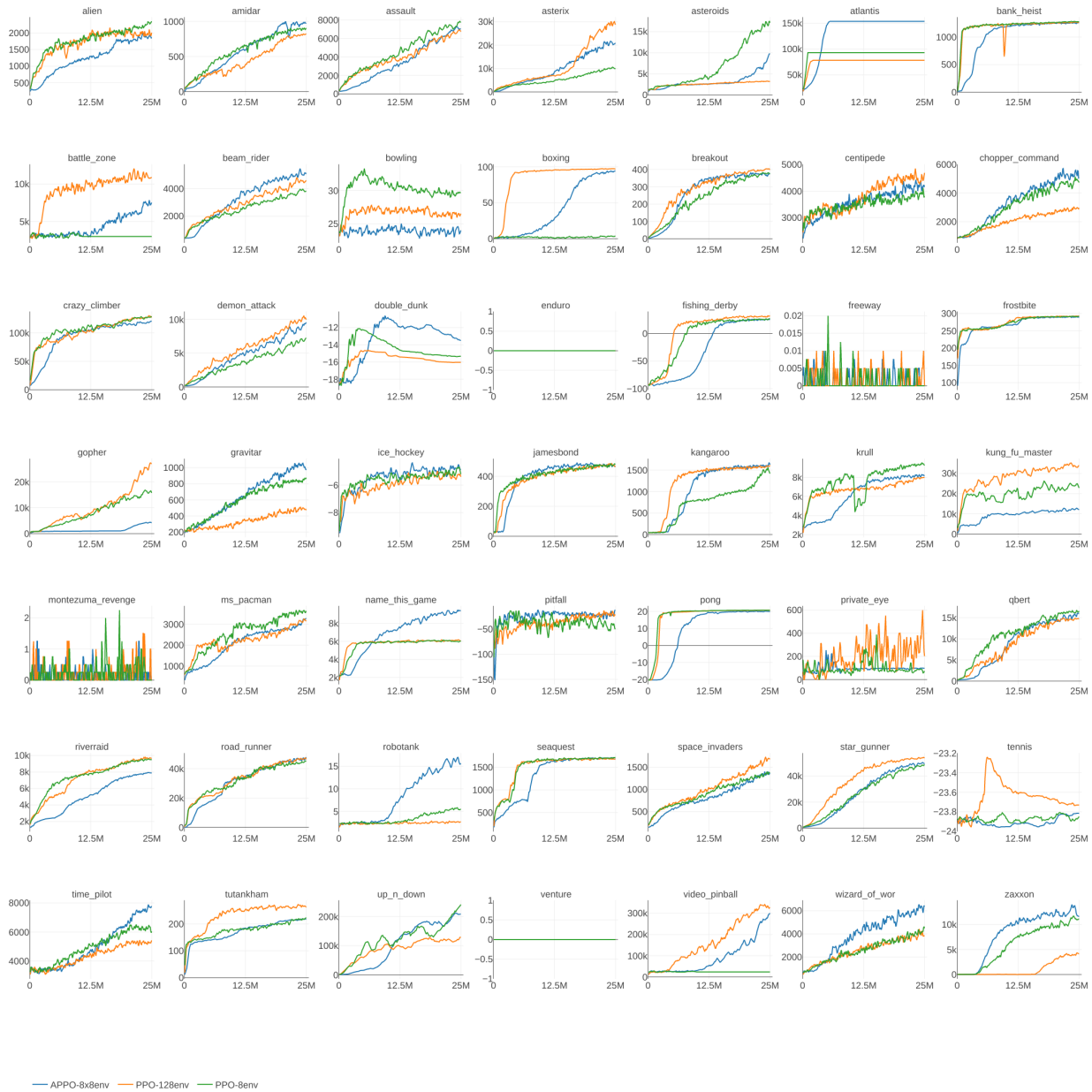


Figure 11. Learning curves for Proximal Policy Optimization: baseline (PPO-8env) and scaled configurations, including synchronous and asynchronous. Only in ASTEROIDS and BOWLING does the baseline stand out above both scaled versions.



Figure 12. Learning curves for scaled versions of DQN (synchronous only): DQN-512, Categorical-DQN-2048, and ϵ -Rainbow-512, where the number refers to training batch size. The anomalously low scores for ϵ -Rainbow in BREAKOUT also appeared for smaller batch sizes, but was remedied when setting the reward horizon to 1 or with asynchronous optimization (cause unknown; reward horizon 3 usually helped).